Supporting Information for "Stretching and Controlled Motion of Single-Stranded DNA in Locally-Heated Solid-State Nanopores"

Maxim Belkin, Christopher Maffeo, David B. Wells and Aleksei Aksimentiev*

E-mail: aksiment@illinois.edu

Simulation Methods

All-atom simulations of single-stranded DNA in a uniformly heated bulk solution. The single-stranded DNA molecule used in our nanopore simulations was also simulated in a uniformly heated bulk solution. To prepare the simulation system, the 54-nucleotide DNA strand was solvated in a volume of pre-equilibrated water molecules. K^+ and Cl^- ions were added to produce a neutral 1 M solution. The system was then equilibrated in the NPT ensemble for 6 ns; the mean dimensions of the system during the last 4 ns of equilibration were used in the production NVT simulations. Equilibration steps were repeated for the following temperatures: 295 K, 350 K, 400 K, and 500 K. Compared to the 295 K system, the total volume of the 350 K, 400 K, and 500 K systems increased

*To whom correspondence should be addressed

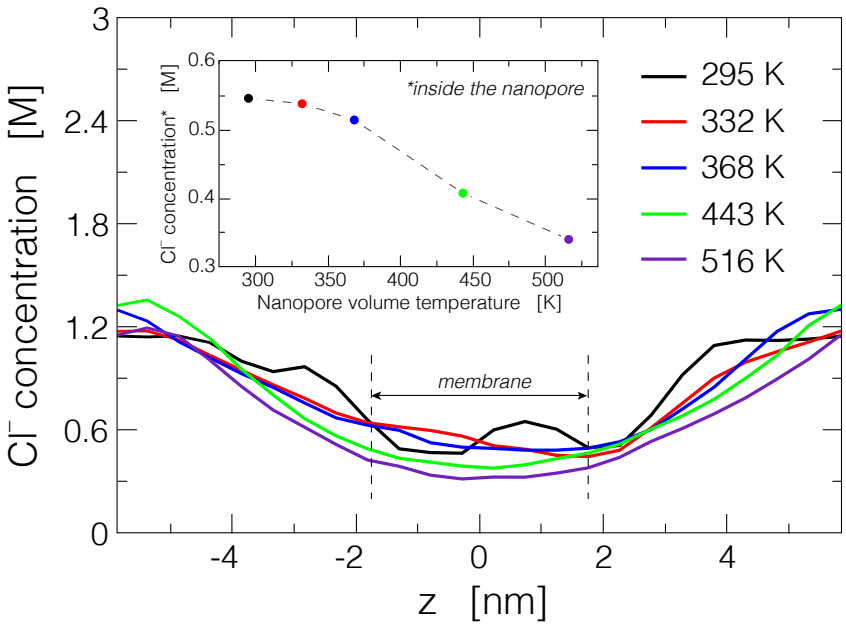

Figure S1: Ion concentration in locally heated nanopore systems. The local molar concentration of Cl^- ions is plotted along the axis of the nanopore for several values of the nanopore temperature. Vertical dashed lines indicate the location of the Si_3N_4 membrane. *Inset* Average value of Cl^- concentration within the nanopore volume as a function of the volume's average temperature.

by 5.2 %, 11.3 % and 32.9 %, respectively. The resulting dimensions of the final simulation system were sufficient to avoid DNA interactions with its periodic cell images, see Figure S2a.

Coarse-grained model of single-stranded DNA. We developed a simple, bottom-up coarse-grained (CG) model of ssDNA that represents each nucleotide using two isotropic interaction sites: a base (B) bead and a backbone (P) bead. Our parametrization scheme relied on Boltzmann inversion of distributions obtained from all-atom simulations, taking into account the presence of solvent implicitly.

To derive the bonded parameters of the CG model, a 1.3 μs all-atom simulation was performed in the NPT ensemble on a system containing a 60-nucleotide poly(dC) strand submerged in an

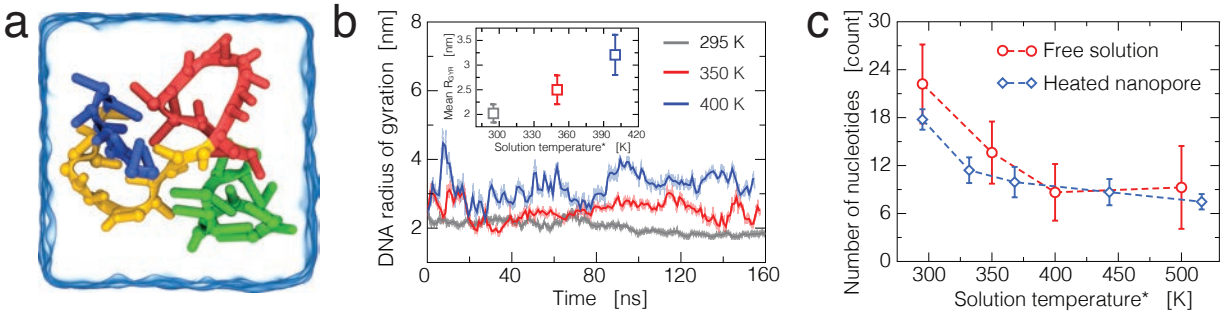

Figure S2: MD simulations of single-stranded DNA in bulk solutions of different uniform temperatures. (a) Representative conformation of a DNA strand in a simulation performed at T = 332 K. The DNA strand is colored to reflect its nucleotide sequence (blue adenine, yellow cytosine, red thymine and green guanine); the solvent is shown as a semitransparent surface. (b) Radius of gyration of the DNA strand in MD simulations of several bulk solution systems. (c) Average number of DNA nucleotides within 17.5 Å of the center of mass of the DNA strand in bulk solution simulations as a function of the solution temperature. For comparison, the number of nucleotides within 17.5 Å of the geometrical center of the Si_3N_4 nanopores (heated nanopore simulations) is plotted *versus* the average temperature of the solution inside the nanopore.

$80\times80\times80$ Å^3 box of 100 mM NaCl solution. The resulting all-atom trajectory was subsequently converted into a CG representation. For a given nucleotide, the P bead represented the O5T′, O5′, P, O1P, O2P, C5′ atoms of that nucleotide and the C3′ O3′ atom of the adjacent nucleotide such that the bead was roughly centered on the phosphorous group of the DNA backbone. The remaining atoms of the nucleotide were converted onto the B bead. For both types of beads, the conversion procedure was done by computing the center of mass of the respective groups of atoms; hydrogen atoms were neglected during the conversion procedure.

The distributions of bond length between P_n and B_n beads and two adjacent P_n and P_{n+1} beads (subscripts refer to the nucleotide number in the all-atom model) were very sharp, exhibiting a single peak of $\sim$1 Å width. Using the Boltzmann inversion procedure, the corresponding bond-length potentials could be easily approximated by a harmonic potential. However, both B_n–P_n–P_{n+1} and P_{n-1}–P_n–P_{n+1} angle distributions were quite broad. The corresponding angle potentials

were tabulated with 1° resolution and applied in a CG MD simulation *via* a custom TCL forces script.[1] Various dihedral distributions were examined and found to span the conformational space evenly and hence were excluded from our model.

To parametrize the non-bonded interactions between the beads, we simulated a system of twelve 5′-phosphorylated, poly(dC)$_5$ fragments using the all-atom MD method. In this simulation, the numbers of water molecules, ions and nucleotides, as well as all other simulation parameters, were the same as in our simulations of the 60-nt system described above. The use of short oligonucleotides increased sampling of non-bonded interaction. The obtained all-atom MD trajectory was converted into a CG representation. The distribution functions for all pairs of P and B beads of the central nucleotide of each fragment were obtained. The iterative Boltzmann inversion (IBI) scheme[2] was applied to determine the non-bonded CG potentials. The resulting potentials were used to describe the non-bonded interactions between two P beads, two B beads and P and B beads. These interactions were implemented in NAMD as tabulated potentials; 1-2 exclusion of non-bonded forces applied.

Our CG model of ssDNA was validated by performing equilibrium CG MD simulation of ssDNA of various lengths. The simulated dependence of the radius of gyration, R_g, of ssDNA on the length of ssDNA was compared with the experimental dependence obtained by means of small-angle X-ray scattering,[3] Figure S3a. The simulated R_g values were found to be less than 15% smaller than the experimental values at 1 M NaCl.

Another validation of our CG model was a simulation of the force-extension dependence of a 200-nucleotide ssDNA fragment. In these CG MD simulations, two forces equal in magnitude and opposite in direction were applied to the terminal P beads of the DNA strand, stretching the strand. Figure S3b compares the results of such CG MD simulations with the experimental data.[4]

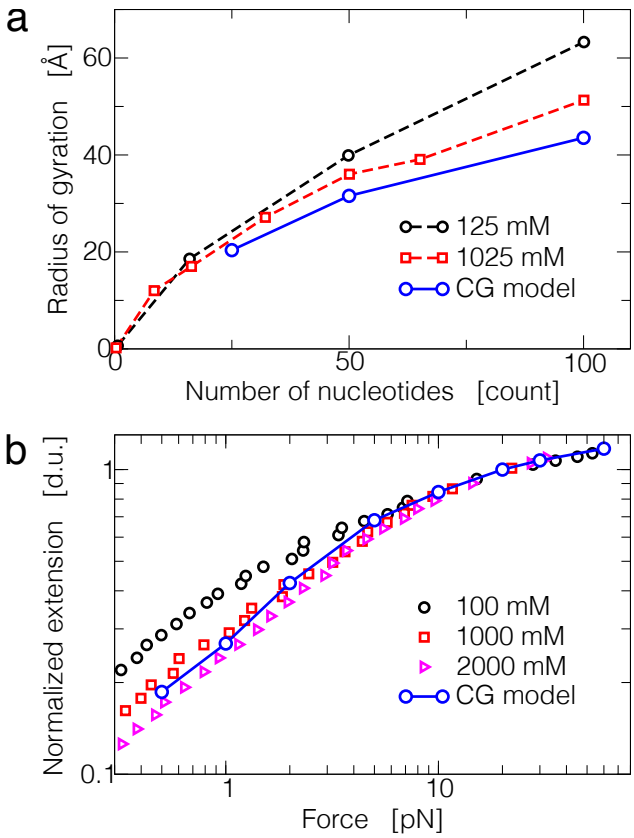

Figure S3: Validation of the CG model. (a) Comparison of the experimentally-measured radius of gyration of poly(dT)[3] (black circles, red squares) and the simulated radius of gyration (large blue circles). (b) Comparison of the experimental force-extension curves[4] (black circles, red squares, magenta triangles) and the simulated force-extension curve (large blue circles). For each data point, the extension value was scaled by the extension under a 20 pN force. Since the absolute values of the extension were not reported in the experimental study,[4] direct comparison of absolute extensions was not possible.

The results of our validation simulation demonstrate good agreement between the simulated and measured force-extension curves at 1 M NaCl, which justifies the use of our CG model in the present study.

Coarse-grained simulations of ssDNA in a locally heated nanopore system. The CG model of ssDNA was used to evaluate the effect of thermophoresis on a long ssDNA molecule threaded through a locally heated nanopore system. In our CG MD system, the nanopore had the same

dimensions as in our all-atom MD system, however the membrane dimensions and the volume of the entire simulation system were considerably greater than those of the corresponding all-atom system: the CG system was $\sim$100 nm on each side.

The presence of a membrane in our CG MD simulations was taken into account by means of a grid-based steric exclusion potential.[5] This 2 Å resolution grid potential was set to 20 $k_{\mathrm{B}}T$ within the volume of the membrane and 0 more than 2 Å away from the membrane surface. The force due to the temperature gradient was described using another grid-based potential (5 Å resolution) derived from the COMSOL solution of the continuum model of the locally-heated nanopore system, Figure 1a. The effective thermophoretic force was assumed to linearly depend on the local temperature gradient. The local values of the effective force were computed based on the value obtained in our all-atom MD simulations: 0.3 pN per nucleotide for a temperature gradient of 100 K over 80 Å, Figure 3. In the CG MD simulations, the thermophoretic force was split equally between the P and B beads of each nucleotide.

All CG MD simulations were performed using a 20 fs timestep and a 49 Å cutoff for non-bounded interactions between the DNA beads. The coordinates of the beads were recorded every 1000 simulation steps. To assess the physical time scale of our CG MD simulations, we simulated electrophoretic motion of a 54-nucleotide DNA strand using both CG and all-atom MD methods under the same external electric field. The simulation revealed approximately 10-fold difference in the velocity of the DNA motion, suggesting that a 1μs CG MD simulation corresponds to $\sim$10 μs of all-atom MD.

In our CG MD simulations of locally heated nanopore systems, one of the DNA ends was harmonically restrained to a point in the center of the nanopore (the spring constant was 2 kcal/(mol·Å^2)). The restraining potential acted only along the pore axis; the motion within the plane of the mem-

brane was not restrained by the harmonic potential (but was restrained by the steric exclusion potential mimicking the action of the membrane). The displacement of the restrained DNA end along the pore axis reported the effective force applied to the strand. Four DNA lengths (125, 250, 500 and 1000 nucleotides) and four heating conditions (ΔT = 0, 35, 65, and 100 K) were tested. The results are shown in Figure 4c of the main text. To obtain statistically significant values, twelve replicas of each systems were simulated in parallel for $\sim$1.5 μs each. The effective thermophoretic force was averaged over the last 200 ns of each trajectory and over the twelve replicas.

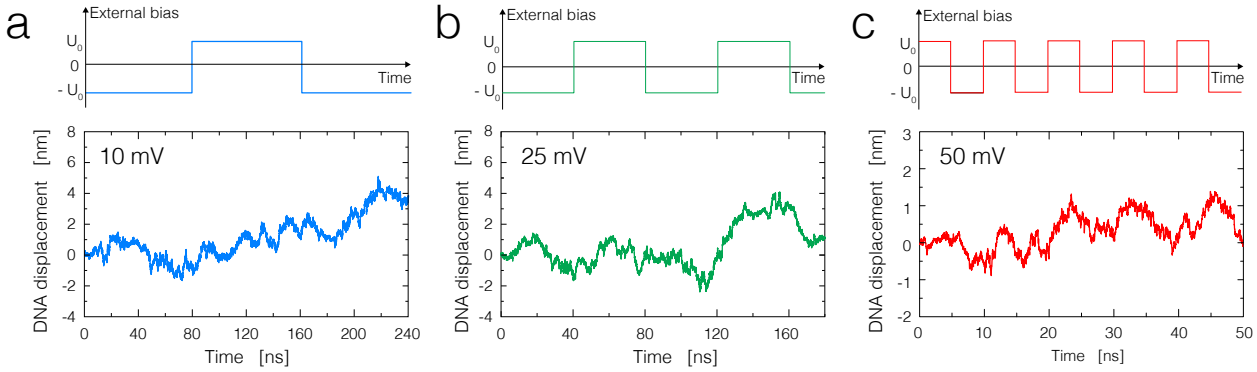

Figure S4: Electrophoretic motion of DNA through a nanopore assisted by local heating. (a-c) Displacement of ssDNA through the nanopore in MD simulations performed under alternating electric field. In each panel, the top row shows the time dependence of the transmembrane bias; the magnitude of the bias is 10, 25 and 50 mV in panels a, b, and c, respectively. In all simulations, the temperature of the heater element was 400 K; the temperature of the nanopore volume $T_{\mathrm{n.v.}}$ = 368 K.

Analysis of the MD trajectories

Temperature distribution in all-atom systems. To compute the distribution of temperature in our all-atom systems, velocities of all atoms in the system were recorded every 9.6 ps along with their coordinates. The instantaneous temperature in a particular subvolume was computed as: T = 2 K / (N_{DOF} k_{B}), where K is the total kinetic energy of all atoms in that volume, N_{DOF} is the number of degrees of freedom of all atoms in that volume and k_{B} is the Boltzmann constant. Although stable temperature gradients established in our systems within $\sim$ 1 ns, we typically performed averaging over 10 ns intervals. In our analysis of the thermophoretic force simulations (Figure 3), the temperature was calculated using 5 Å layers arranged perpendicular to the z-axis. Analysis of the solid-state nanopore systems was performed using cubic bins with $\sim$ 5 Å-long sides. To plot the temperature profile through the nanopore (Figure 1c), we used data from the bins that the nanopore axis passed through.

Number of nucleotides. To determine the number of DNA nucleotides confined in a nanopore, the number of atoms inside the nanopore was determined for each nucleotide and then divided by the total number of atoms in that nucleotide. Atoms were considered to reside inside the nanopore if their coordinates satisfied the condition: -17.5 $<$ z $<$ 17.5 Å, where the top and bottom surfaces of the membrane are located at z = 17.5 Å and z = -17.5 Å, correspondingly. Obtained fractions across all nucleotides were then added up to yield the aggregate number of nucleotides in the nanopore, $\mathrm{N_{n.v.}}$.

To quantitatively compare conformations of DNA in the heated nanopore and free solution simulations, for both types of the simulations we computed the number of nucleotides confined in a spherical volume of 17.3 Å radius, N_{sp}. In the case of the heated nanopore simulations, the

volume's center was in the middle of the nanopore. In the case of the free solution simulations, the volume's center was at the center of mass of the DNA fragment. Comparison between $N_{n.v.}$ to N_{sp} is shown in Figure S2c.

Ion concentration profile. Figure S1 shows the profile of Cl^- molar concentration in our solid-state nanopore systems. To compute the concentration profiles, the system was split into ~ 5 Å-thick 12 Å-radius cylindrical slabs along the z axis. The number of ions within each slab was averaged over the corresponding MD trajectory and divided by the volume of the slab. The radius of the cylindrical slabs was chosen to minimize the effect of specific ion–nanopore surface interactions while providing statistically significant number of ion observations.

DNA mobility and translocation velocity. To compute the velocity of DNA translocation through a nanopore, the velocity of each nucleotide in the nanopore was computed as displacement of its center of mass divided by the time during which this displacement occurred. Instantaneous velocity of DNA translocation $v_{DNA}(t)$ through the solid-state nanopore was taken as the average velocity of all nucleotides confined inside the nanopore, *i.e.* nucleotides whose centers of mass satisfied the condition $-17.5 < z < 17.5$ Å. Reported in Figure 5, DNA displacement was then computed as:

$$L(t) = \int_0^t v_{DNA}(\tau)\mathrm{d}\tau. \tag{1}$$

The average velocity of DNA translocation was extracted from a linear fit to the plot of the DNA displacement. Electrophoretic mobility of DNA was then readily calculated as the translocation velocity divided by the applied electric field. In our analysis of the simulations employing an alternating electric field, we first combined traces corresponding to the same direction of the applied

field into one before proceeding as described above.

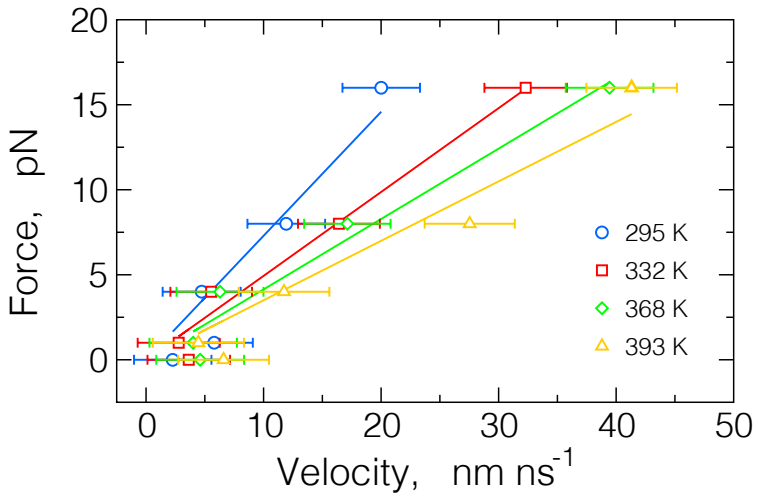

Figure S5: The effect of temperature on water viscosity probed by all-atom molecular dynamics simulations. In each simulation, two water molecules (randomly selected from a 47.5^3 Å^3 volume of bulk water) were pulled in opposite directions by applying same-magnitude opposite-direction forces. The resulting displacements of the molecules were used to determine the average terminal velocity of the molecules. The slopes of the linear fits to the data are proportional to water viscosity.

Temperature dependence of water viscosity. To determine how viscosity of the employed water model depends on temperature, we simulated a box of water at 4 temperature values: 295, 332, 368, and 393 K. Initial volumes of all system were identical and equal to 47.5^3 Å^3 containing 3,332 water molecules. Following 1,000 steps of energy minimization, each system was then equilibrated in the NPT ensemble for 2.4 ns. During this equilibration, a Lowe-Andersen[6] thermostat maintained desired temperature, while Nosé-Hoover Langevin piston pressure control[7] maintained the pressure of 1 atm. Using the TclForces feature of NAMD we then pulled two water molecules with equal and constant forces (1, 4, 8 and 16 pN) in opposite directions and determined their terminal velocities from 1 ns-long simulations. The average of the terminal speeds of the two molecules was then found to eliminate the impact of system drift. Figure S5 shows the relationship between

the applied force and the average terminal speed of the water molecules. The slope of the linear fits, $|\mathbf{F}| = \alpha|\mathbf{v}|$, decrease with increasing temperature and equal to 0.729 at 295 K, 0.493 at 332 K, 0.414 at 368 K and 0.350 at 393 K. Assuming the water viscosity is proportional to the slopes of the linear fits, the water viscosity decreases by a factor of 2 when the temperature of the system increases from 295 to 368 K.

Single-file character of DNA conformation in a nanopore. In all our simulation systems, the nucleotides were numbered in ascending order starting from the 5′-end of the strand. We considered a DNA strand to have a single-file conformation if the center-of-mass coordinates of the DNA nucleotides monotonically increase as one moves in the 5′ to 3′ direction along the fraction of the DNA strand confined in the nanopore. Specifically, for each frame of the MD trajectory, we first selected all nucleotides whose atoms resided within a 1-nm-thick section of the nanopore volume, $|z| < 0.5$ nm. Next, the nucleotides closest and furthers to the 5′ end of the strand (nucleotides m and n) were identified among the selected nucleotides. If $z_m \leq z_{m+1}, \ldots, \leq z_n$, the DNA conformation was classified as single-file. Figure 6 of the main text reports the percentage of single-file conformations within the specified MD trajectories.

Animations of MD trajectories

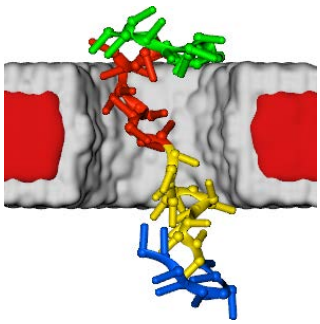

Animation M1: Unwinding of a single-stranded DNA in a locally heated Si_3N_4 nanopore. The Si_3N_4 membrane is shown in gray; the DNA molecule is shown in balls and sticks representation and colored to reflect its nucleotide sequence (blue adenine, yellow cytosine, red thymine and green guanine). The heated region of the membrane (shown in red) is kept at ΔT = 100 K higher than the ambient temperature, producing the temperature increase in the nanopore volume of $\sim$70 K. The animation shows 20 ns of all-atom MD simulation.

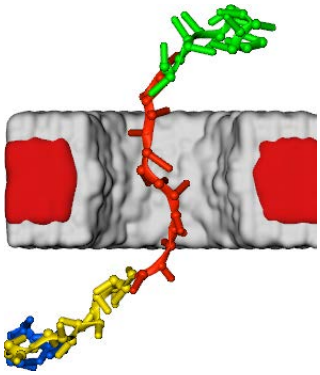

Animation M2: Relaxation of a single-stranded DNA molecule following the unwinding simulation illustrated by Animation M1. In this simulation, the heating source was switched off. The Si_3N_4 membrane is shown in gray; the DNA molecule is shown in balls and sticks representation and colored to reflect its nucleotide sequence (blue adenine, yellow cytosine, red thymine and green guanine). The animation covers $\sim$ 200 ns of all-atom MD simulation.

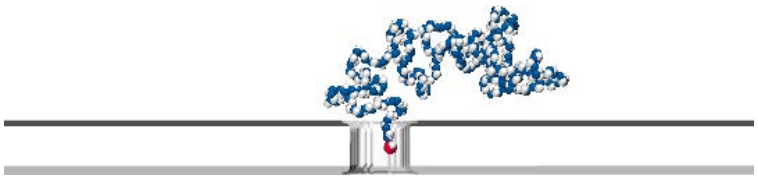

Animation M3: Coarse-grained MD simulation of a 250-nucleotide ssDNA fragment in a locally heated nanopore system. No heating was applied in this simulation. One end of the DNA strand is restrained to the center of the nanopore, the force of the restrain reports the effective force on the strand. The membrane is shown in gray, DNA molecule is shown by blue and white spheres for the backbone and base beads, correspondingly, and the restrained backbone atom is shown as a red sphere. The animation covers 1.0 μs of CG MD simulation, which corresponds to $\sim$ 10 μs of physical time.

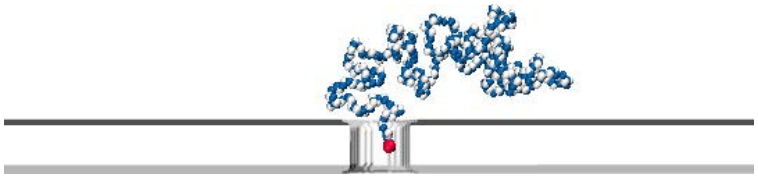

Animation M4: Coarse-grained MD simulation of a 250-nucleotide ssDNA fragment in a locally heated nanopore system. The local heater element temperature was set to be 100 K higher then the room temperature; the temperature of the solvent in the nanopore volume was $\sim$70 K higher then the room temperature. One end of the DNA strand is restrained to remain in the center of the nanopore, the force of the restraint reports the effective force on the strand. The membrane is shown in gray, DNA molecule is shown in blue and white spheres for the backbone and base beads, correspondingly, and the restrained backbone atom is shown as red sphere. The animation covers 1.27 μs of CG MD simulation, which corresponds to $\sim$12.7 μs of physical time.

References

1. Phillips, J. C.; Braun, R.; Wang, W.; Gumbart, J.; Tajkhorshid, E.; Villa, E.; Chipot, C.; Skeel, R. D.; Kale, L.; Schulten, K. Scalable Molecular Dynamics with NAMD. *J. Comput. Chem.* **2005**, *26*, 1781–1802.

2. Reith, D.; Pütz, M.; Müller-Plathe, F. Deriving Effective Mesoscale Potentials From Atomistic Simulations. *J. Comput. Chem.* **2003**, *24*, 1624–1636.

3. Sim, A.; Lipfert, J.; Herschlag, D.; Doniach, S. Salt Dependence of the Radius of Gyration and Flexibility of Single-Stranded DNA in Solution Probed by Small-Angle X-Ray Scattering. *Phys. Rev. E* **2012**, *86*, 1–5.

4. Saleh, O.; McIntosh, D.; Pincus, P.; Ribeck, N. Nonlinear Low-Force Elasticity of Single-Stranded DNA Molecules. *Phys. Rev. Lett.* **2009**, *102*, 068301.

5. Wells, D. B.; Abramkina, V.; Aksimentiev, A. Exploring Transmembrane Transport through α-Hemolysin with Grid-Steered Molecular Dynamics. *J. Chem. Phys.* **2007**, *127*, 125101.

6. Koopman, E.; Lowe, C. Advantages of a Lowe-Andersen Thermostat in Molecular Dynamics Simulations. *J. Chem. Phys.* **2006**, *124*, 204103.

7. Martyna, G. J.; Tobias, D. J.; Klein, M. L. Constant Pressure Molecular Dynamics Algorithms. *J. Chem. Phys.* **1994**, *101*, 4177–4189.